0026-895X/09/7503-514–524$20.00
MOLECULAR PHARMACOLOGY
Vol. 75, No. 3
48744/3443845
Mol Pharmacol 75:514–524, 2009
Printed in U.S.A.

A Juxtamembrane Mutation in the N Terminus of the Dopamine Transporter Induces Preference for an Inward-Facing Conformation

Bipasha Guptaroy, Minjia Zhang, Erica Bowton, Francesca Binda, Lei Shi, Harel Weinstein, Aurelio Galli, Jonathan A. Javitch, Richard R. Neubig, and Margaret E. Gnegy

Department of Pharmacology, University of Michigan, Ann Arbor, Michigan (B.G., M.Z., R.R.N., M.E.G.); Department of Pharmacology and Psychiatry, Center for Molecular Recognition, College of Physicians and Surgeons, Columbia University, New York (J.A.J.); Department of Physiology and Biophysics and the HRH Prince Alwaleed Bin Talal Bin Abdulaziz Alsaud Institute for Computational Biomedicine, Weill Cornell Medical College, Cornell University, New York (L.S., H.W.); and the Department of Molecular Physiology and Biophysics, Center for Molecular Neuroscience and Kennedy Center, Vanderbilt University, Nashville, Tennessee (E.B., F.B., A.G.)

Received May 12, 2008; accepted December 12, 2008

ABSTRACT

The human dopamine transporter (hDAT) regulates synaptic dopamine (DA) levels and is the site of action of abused and therapeutic drugs. Here we study the effect of a threonine residue (Thr62 in hDAT) that is highly conserved within a canonical phosphorylation site (RETW) in the juxtamembrane N-terminal region of monoamine transporters. In stably transfected human embryonic kidney 293T cells, expression of T62D-hDAT was reduced compared with hDAT or T62A-hDAT. T62D-hDAT displayed dramatically reduced [^{3}H]dopamine uptake but exhibited a higher basal dopamine efflux compared with hDAT or T62A-hDAT, as determined by measurements of [^{3}H]dopamine efflux and amperometry. The high constitutive efflux in T62D-hDAT precluded the measurement of amphetamine-stimulated [^{3}H]dopamine efflux, but when dopamine was added internally into voltage-clamped T62D-hDAT cells, amphetamine-induced efflux comparable with hDAT was detected by amperometry. In accordance with findings that Zn^{2+} can rescue reduced DA uptake in mutant transporters that are predominantly inward-facing, micromolar concentrations of Zn^{2+} markedly potentiated [^{3}H]dopamine uptake in T62D-hDAT and permitted the measurement of amphetamine-stimulated dopamine efflux. These results suggest that T62D-hDAT prefers an inward-facing conformation in the transition between inward- and outward-facing conformations. For T62A-hDAT, however, the measured 50% reduction in both [^{3}H]dopamine uptake and [^{3}H]dopamine efflux was consistent with a slowed transition between inward- and outward-facing conformations. The mechanism underlying the important functional role of Thr62 in hDAT activity suggested by these findings is examined in a structural context using dynamic simulations of a three-dimensional molecular model of DAT.

The strength and duration of dopaminergic neurotransmission is tightly controlled by the dopamine transporter (DAT), which mediates reuptake of synaptic dopamine (DA) (Chen and Reith, 2000) and is a target for therapeutic drugs and abused psychostimulants (Sulzer et al., 2005). Amphetamine (AMPH), a substrate for DAT, competitively inhibits DA reuptake and elicits outward transport of DA by reversal of the transporter (Sulzer et al., 2005), purportedly by an exchange diffusion mechanism (Fischer and Cho, 1979; Sulzer et al., 2005). This model assumes that the transporter transitions between two primary conformational states—an "outward-facing" conformation favoring substrate binding and influx, and an "inward-facing" conformation in which the binding sites are available to the intracellular milieu and which favors substrate efflux. In the absence of substrate, the transporter favors an outward-facing conformation ready to bind

This work was supported by the National Institutes of Health National Institute on Drug Abuse [Grants DA11697, DA12408, DA14684, DA022413, DA023694]. This work used the DNA Sequencing Core of the Michigan Diabetes Research and Training Center, supported by the National Institutes of Health National Institute of Diabetes and Digestive and Kidney Diseases [Grant 5P60-DK20572].

Article, publication date, and citation information can be found at http://molpharm.aspetjournals.org.

doi:10.1124/mol.108.048744.

ABBREVIATIONS: DAT, dopamine transporter; AMPH, amphetamine; DA, dopamine; HEK, human embryonic kidney; KRH, Krebs-Ringer-HEPES; PKC, protein kinase C; PKA, cAMP-dependent protein kinase; TM, transmembrane domain; ANOVA, analysis of variance; cGPK, cGMP-dependent protein kinase; MD, molecular dynamics; FEP, free energy perturbation; GBR12935, 1-[2-(diphenylmethoxy)ethyl]-4-(3-phenylpropyl)-piperazine; IL, intracellular loop.

extracellular substrate and assume an inward-facing conformation (Sulzer et al., 2005). After dissociation of inwardly transported AMPH, the transporter binds intracellular substrate and reverses its conformation to cause efflux. This predicts that the influx and efflux rates would be modified equivalently. However, recent studies demonstrate that influx and efflux of substrates through the transporter can be modulated independently (Kantor and Gnegy, 1998; Sitte et al., 1998; Pifl et al., 1999; Chen and Justice, 2000; Khoshbouei et al., 2004).

The molecular structure of human DAT (hDAT) comprises 12 transmembrane (TM) segments with cytoplasmic N and C termini and a large second extracellular loop with several putative *N*-glycosylation sites (Giros and Caron, 1993). The N-terminal region of the transporter and the first transmembrane domain are important for substrate binding and function of the transporter. Based on the crystal structure of the bacterial leucine transporter ($LeuT_{Aa}$) (Yamashita et al., 2005) and subsequent structure-based alignment for DAT (Beuming et al., 2006), TM1 is predicted to have a "break" in its helical structure in the membrane bilayer that comprises part of the substrate binding site. The N-terminal cytoplasmic region of DAT is a site for phosphorylation (Foster et al., 2002) and for the binding of proteins involved in phosphorylation, such as syntaxin 1A, whose function is regulated by phosphorylation, and receptor for activated C kinase 1, which facilitates phosphorylation (Torres, 2006). Phosphorylation of serines within the N-terminal region seems to maintain normal AMPH-stimulated DA efflux (Khoshbouei et al., 2004). Mutating other serine and threonine residues in the DAT N terminus alters the ability of various kinase-modulating drugs to regulate DAT function and expression (Lin et al., 2003).

Considerable information concerning DAT structure and function relationships come from site-directed mutagenesis studies. Most studies have focused on the TM domains that are highly conserved between the transporters and across species and probably contribute to the "binding pocket" involved in substrate and antagonist recognition and substrate translocation (Uhl and Lin, 2003). Mutations of residues in regions outside of these domains, such as distal TMs (Kitayama et al., 1992; Wu and Gu, 2003; Sen et al., 2005), extracellular (Uhl and Lin, 2003) and intracellular loops (Loland et al., 2002; Chen et al., 2004; Loland et al., 2004), and the N- and C-terminal domains (Lee et al., 1996; Khoshbouei et al., 2004), also affect transporter function. The relationship of these sites to the structure of DAT was clarified (Beuming et al., 2006) in the context of three-dimensional structural information for the cognate LeuT (Yamashita et al., 2005).

Here we investigate the effect of mutations of a threonine residue (Thr62) located within a juxtamembrane site (RETW) that is highly conserved in the plasmalemmal transporters for DA, norepinephrine, and serotonin; interestingly, it is within a canonical site for PKC/cGMP-dependent protein kinase (cGPK)/PKA-dependent phosphorylation (Giros and Caron, 1993; Granas et al., 2003). In rat DAT, the mutation of this site to alanine alters the actions of some kinase effectors (Lin et al., 2003). We investigated whether mutation of this highly conserved residue to alanine, a somewhat conservative substitution, or a nonconservative substitution to aspartate, would alter DAT function. These mutations mimic a nonphosphorylatable state (alanine) or a phosphorylated state (aspartate), addressing the putative role of phosphorylation at this site (Thorsness and Koshland, 1987). We find a profound change in the balance of influx and efflux in the Thr62 to aspartate mutant with less dramatic, but still altered, effects upon mutation to alanine. These results support the importance of the TM1-juxtamembrane N-terminal region in regulating transporter function.

Materials and Methods

Mutagenesis and Generation of Stable Cell Lines. A synthetic hDAT cDNA, tagged at the N terminus with a FLAG epitope, was used in these studies. The gene encodes a protein with an amino acid sequence identical with wild-type human DAT, but the nucleotide sequence was altered to increase the number of unique restriction sites and optimize codon use (Saunders et al., 2000). The cDNA was cloned into a bicistronic vector pCIHyg (Saunders et al., 2000) derived from pIREShyg vector from Clontech (Mountain View, CA). Previous studies have shown that the addition of the N-terminal FLAG tag does not alter transporter function (Saunders et al., 2000). Mutations were made by polymerase chain reaction and confirmed by sequencing. In brief, sense and antisense mutagenic oligonucleotides were synthesized and used for polymerase chain reaction to synthesize mutagenized DNA using Vent DNA polymerase (Promega Corporation, Madison, WI). Methylated parental DNA strands in the sample were digested using DpnI enzyme (Promega, Madison, WI) for 2 h at 37°C, and these were then transformed into XL10-Gold competent cells (Stratagene, La Jolla, CA). Clones were analyzed by DNA sequencing. The cDNAs for hDAT and mutants were stably transfected into HEK 293T cells with Lipofectamine (Invitrogen, Carlsbad, CA), and a stable pool of hygromycin-resistant cells was selected. Cells were maintained in Dulbecco's modified Eagle's medium supplemented with 10% fetal bovine serum at 37°C and 5% CO_2.

Cell Surface Biotinylation. Surface expression of the wild-type and mutant transporters in HEK 293T cells was determined by reacting the surface proteins in suspension with sulfosuccinimidyl-2-(biotinamido)ethyl-1, 3-dithiopropionate (sulfo-NHS-SS-biotin) (Pierce, Rockford, IL) at 4°C as described previously (Johnson et al., 2005). The reaction was attenuated by incubating the biotinylated cells with 100 mM glycine at 4°C. Cells were lysed in solubilization buffer (25 mM Tris, 150 mM NaCl, 1 mM EDTA, 5 mM *N*-ethylmalemeide, phenylmethylsulfonyl fluoride, and 1% Triton X-100) containing protease inhibitors (Roche, Indianapolis, IN) and centrifuged at 20,000*g* to remove cell debris. Lysates containing 700 μg of protein were incubated with 50 μl of monomeric Streptavidin beads (Pierce) for 1 h at room temperature. Beads were washed four times with radioimmunoprecipitation assay buffer and then eluted in 2× SDS-polyacrylamide gel electrophoresis sample buffer containing dithiothreitol and resolved by electrophoresis on a 10% Tris-glycine gel.

Immunoblot Analysis. To detect hDAT, proteins were transferred to a nitrocellulose membrane after electrophoresis on SDS polyacrylamide gel. Membranes were blocked with Tris-buffered saline/Tween 20 (10 mM Tris, pH 7.4, 150 mM NaCl, and 0.1% Tween 20) containing 5% milk for 1 h followed by overnight incubation with anti-DAT antibody, monoclonal antibody 369 (Millipore Bioscience Research Reagents, Temecula, CA) at a 1:1000 dilution in 5% milk, followed by three rinses with Tris-buffered saline/Tween 20. Membranes were then incubated with goat anti-rat secondary antibody (Santa Cruz Biotechnology, Santa Cruz, CA) at 1:5000 dilution (0.08 μg/ml), followed by washes as before. Chemiluminescence was detected by enhanced chemiluminescence (GE Healthcare, Chalfont St. Giles, Buckinghamshire, UK). Quantification of bands was done by densitometry using Scion Image software (Scion Corporation, Frederick, MD). We normalized to loading equal protein for each lane, along with total transporter, and in some experiments, actin was

used as an internal control, which remained unchanged among the samples.

Uptake of [^{3}H]DA. For time course experiments measuring the initial rate of [^{3}H]DA uptake, cells were plated on 24-well plates at 100,000 cells/well. On the following day, cells were rinsed with KRH (25 mM HEPES, pH 7.4, 125 mM NaCl, 4.8 mM KCl, 1.2 mM KH_2PO_4, 1.3 mM $CaCl_2$, 1.2 mM $MgSO_4$, and 5.6 mM glucose), and [^{3}H]DA uptake was measured in the absence or presence of 10 μM GBR12935 (Sigma, St. Louis, MO). Uptake was initiated with [^{3}H]DA (specific activity, 59.3 Ci/mmol; PerkinElmer Life and Analytical Sciences, Waltham, MA) in concentrations ranging from 30 nM to 3 μM in a final volume of 250 μl and allowed to proceed for 0 to 2 min at room temperature and was stopped by rapidly washing the cells three times with cold phosphate-buffered saline. Cells were solubilized in 1% SDS, and radioactivity was counted using Scintiverse BD (Thermo Fisher Scientific, Waltham, MA) in a Beckman LS 5801 liquid scintillation counter (Beckman Coulter, Fullerton, CA). For assaying [^{3}H]DA uptake in the presence of AMPH (Sigma), cells were incubated with 30 nM [^{3}H]DA and varying concentrations of AMPH (10 nM to 3 μM) for 10 min and then assayed as described above. Nonspecific uptake was measured in the presence of 10 μM GBR12935. Uptake in the presence of Zn^{2+} was determined using 15 nM [^{3}H] DA for 10 min at ambient temperature after preincubation with Zn^{2+}.

[^{3}H]DA Efflux. For measurement of the initial rate of efflux, cells were plated on 12-well plates at a density of 150,000 cells/well. Cells were washed with KRH and incubated with 60 or 120 nM [^{3}H]DA and unlabeled DA at concentrations from 1 to 80 μM for 30 min at room temperature in KRH. The cells were then quickly washed three times with KRH, and 500 μl of KRH was added to the cells and immediately removed for a 0 time point. At additional times (10–30 s), 500-μl aliquots were removed, and KRH was replaced. Finally, cells were lysed in 1% SDS and counted using Scintiverse. Specific efflux was determined in the absence and presence of 100 μM cocaine. For the measurement of basal efflux and AMPH-stimulated DA efflux, cells were plated on 24-well plates at a density of 100,000 to 150,000 cells/well, washed, and loaded with DA for 20 min at room temperature in KRH containing between 0.5 and 5 μM DA, 30 nM [^{3}H]DA, 1 mM tropolone (Sigma), and 100 μM pargyline (Sigma). After three quick washes with KRH, 250-μl aliquots were taken for counting and replaced with fresh KRH every 10 min for 30 min to establish a baseline. At 30 min, 250 μl of AMPH (1–10 μM) was added, and another 250-μl aliquot was taken after 5 min. Finally, cells were lysed in 1% SDS and counted using Scintiverse. Cells from one well were lysed immediately after DA loading to obtain an estimate of the initial amount of DA (total DA) in the cells.

DA Efflux by Superfusion. Confluent 100-mm plates of cells were washed twice with KRH and incubated at 37°C with 5 μM DA for 30 min to load with DA. The hDAT cells were loaded in the absence of Zn^{2+}, and T62D-hDAT cells were loaded in the presence of 30 μM Zn^{2+}. After incubation, cells were washed with KRH, harvested, and resuspended in KRH with or without Zn^{2+}. DA efflux was measured in the eluate of superfused cells. Cells were placed on a Whatman GF/B filter (Whatman, Clifton, NJ) in a chamber of a Brandel superfusion apparatus (Brandel SF-12, Gaithersburg, MD) at room temperature and perfused using KRH with or without Zn^{2+} at 400 μl/min, and 2-min fractions were collected after washing cells for 1 h. AMPH (10 μM) was added and perfused for 2 min followed by KRH for 15 min. Fractions were collected into vials containing 2-amino phenol (Sigma) as an internal standard. Samples were stored at −70°C, and DA content was measured by high-pressure liquid chromatography with electrochemical detection. DA efflux was quantified as the peak DA in the eluent.

Electrophysiology. HEK 293T cell lines stably transfected with T62D-hDAT, T62A-hDAT, and hDAT were used for electrophysiological recordings. Cells were plated 2 days before experiments on 35-mm dishes. For nonclamped amperometric experiments, cells were washed twice with KRH assay buffer (130 mM NaCl, 1.3 mM KCl, 2.2 mM $CaCl_2$, 1.2 mM $MgSO_4$, 1.2 mM KH_2PO_4, 10 mM HEPES, pH 7.4, 10 mM D-glucose, 100 μM pargyline, 10 μM tropolone, and 100 μM ascorbic acid) and were then incubated with 1 μM DA in assay buffer for 45 min at 37°C to actively load the cells with DA. Plates were then washed twice with bath solution (130 mM NaCl, 10 mM HEPES, 34 mM dextrose, 1.5 mM $CaCl_2$, 0.5 mM $MgSO_4$, and 1.3 mM KH_2PO_4 adjusted to pH 7.35) at room temperature. A carbon-fiber electrode (ProCFE; fiber diameter is 5 μm; Dagan Corporation, Minneapolis, MN) touching the plasma membrane of the cell and held at +700 mV with respect to the bath ground (a potential greater than the oxidizing potential of DA) was used to measure DA flux through oxidation reactions. The amperometric electrode measures electrical currents (in picoamperes) as a result of DA molecule oxidation which, after integration, can be converted when required to the number of DA molecules. The amperometric electrode measures the number of DA molecules oxidized and not the concentration of DA. Amperometric currents were then recorded using Axopatch 200B with a low-pass Bessel filter set at 100 Hz and digitally filtered offline at 10 Hz. The cells were not voltage-clamped, allowing the measurement of basal efflux under resting membrane potential conditions. The term "DAT-mediated leak" is used to describe DA efflux under basal conditions of the cell (resting membrane potential) and was defined as amperometric baseline current minus the current present after the addition of 10 μM cocaine (Sigma), a blocker of DAT function. The dotted horizontal lines in Fig. 4 represent the amperometric currents recorded after the addition of cocaine when we had achieved the maximum DAT blockade. Data were acquired by averaging a 15-s interval of current directly before cocaine application (baseline current) and 20 min after cocaine application (cocaine current). The stability of our amperometric signals was confirmed by recording currents with an amperometric electrode positioned in the bath and held at +700 mV for 20 min. When averaged and subtracted as above, the average of the differences was 0.016 ± 0.005 pA (n = 6).

For voltage-clamped experiments, DA efflux was elicited using 30 mM Na^+ and 2 mM DA in the recording pipette (pipette solution: 90 mM KCl, 30 mM NaCl, 0.1 mM $CaCl_2$, 2 mM $MgCl_2$, 1.1 mM EGTA, 10 mM HEPES, 30 mM dextrose, and 2 mM DA, adjusted to pH 7.35) (Khoshbouei et al., 2003). hDAT-, T62D-hDAT-, and T62A-hDAT-mediated effluxes were obtained by subtraction of the efflux value recorded in the presence of 20 μM cocaine from the one recorded in the control condition. Patch electrodes were pulled from quartz pipettes on a P-2000 puller with a resistance of 7 MΩ. Both whole-cell current and amperometric current were recorded from cells. Current-voltage relationships were generated by stepping membrane voltage from a holding potential of −20 mV to voltages between −100 and +100 mV in 20-mV increments for 1 s. Data were recorded and analyzed using pClamp8 software. Current was calculated as the average current during the final 100 ms of the voltage step. For amperometric analysis, a carbon-fiber electrode was used as described above.

Protein Determination. Protein assay was performed according to the Dc protein assay kit (Bio-Rad, Hercules, CA).

Data Analysis. Kinetic constants, including K_m, V_{max}, and IC_{50} values for the hDAT and mutant DAT constructs, were determined by nonlinear regression analysis of the mean values for each mutant using Prism version 5 (GraphPad Software Inc., San Diego, CA). Statistical significance was determined using Prism version 4 either by comparison with hDAT using ANOVA or a two-tailed Student's t test, or with an F test by comparing fits in which selected values were constrained to be equal or were allowed to differ. The null hypothesis was that the best-fit parameter for the value did not differ. A conclusion of statistical significance represents a rejection of the null hypothesis and indicates a difference between designated values.

Molecular Modeling and Simulations. The molecular model for the human DAT was constructed with Modeler 8v2 (Sali and Blundell, 1993) using the LeuT structure as template and the se-

quence alignment detailed in Beuming et al. (2006). As seen from the alignment, the first 59 residues of DAT do not have a corresponding sequence in LeuT, nor do the last 30 residues in the C terminus and 26 residues in the middle of extracellular loop 2. These segments are therefore not included in the DAT model. DAT also has more residues than LeuT in the sixth extracellular loop; these were modeled to continue the helix observed in LeuT. The substrate, dopamine, was positioned in the binding site by aligning the amine group and the hydrophobic portion with those of the substrate in the LeuT structure. The final model also includes two Na^+ ions positioned equivalently to those in LeuT and a Cl^- ion coordinated by residues Asn82, Tyr102, Ser321, and Asn353 of DAT based on the chloride binding site described in Zomot et al. (2007). Before the molecular dynamics (MD) simulation runs, the structure was equilibrated in a model lipid bilayer of 1-palmitoyl,2-oleoyl-*sn*-glycero-3-phosphocholine as described in detail in our recent publication (Shi et al., 2008). In brief, the simulated system composed of the DAT model immersed in an explicit representation of the water/lipid bilayer/water environment was constructed with visual molecular dynamics (Humphrey et al., 1996) and equilibrated with nanoscale molecular dynamics (Phillips et al., 2005) following a procedure modified from Sotomayor and Schulten (2004). During the equilibration of the DAT model in its environment, the backbones were initially fixed and then harmonically constrained, and water was restrained by small forces from penetrating the protein-lipid interface. The constraints were released gradually in three steps of 300 ps each, changing the force constants from 1, to 0.5, and 0.1 kcal/(mol Å^2), respectively. The all-atom CHARMM27 force field was used throughout. Constant temperature (310 K) was maintained with Langevin dynamics, and 1 atm constant pressure was achieved by using the hybrid Nosé-Hoover Langevin piston method on a flexible periodic cell (Shi et al., 2008). The simulated system including the transporter embedded in a membrane patch of 196 1-palmitoyl,2-oleoyl-*sn*-glycero-3-phosphocholine molecules (95 on the periplasmic side and 101 on the cytoplasmic side) and water layers on each side containing Na^+ and Cl^- ions corresponding to a concentration of 150 mM NaCl, is composed of nearly 72,000 atoms in a box with final dimensions (at the end of 16 ns of free equilibration) of $83 \times 89 \times 94$ Å^3.

To model the mutant DAT constructs with T62D and T62A, the mutations were introduced using the free energy perturbation (FEP) method implemented in nanoscale molecular dynamics, which uses the dual-topology paradigm (Henin et al., 2006). Starting from the last snapshot of the constraint-free equilibration of wild-type DAT model, the reaction paths for the gradual transformation of threonine into asparate (or alanine) at the site was divided into 105 stages (windows) of uneven widths, with narrower intermediates states defined toward the end points of the transformation, where the system is more sensitive to the perturbations. Each window in the transformation procedure was run for 40 ps, with the entire transformation accomplished in 4.2 ns.

Results

Surface Expression and Uptake Activity of hDAT and the Thr62 Mutants. Surface expression of the transporter in hDAT-HEK293T (hDAT cells), T62A-hDAT, and T62D-hDAT cells was determined by cell surface biotinylation. A representative blot showing the levels of total and biotinylated surface DAT is shown in Fig. 1A. The overall levels of total and surface expression of the T62A-hDAT and hDAT were comparable (Fig. 1A). However, the surface expression of the T62D mutant was significantly reduced to approximately 50% of hDAT and T62A-hDAT ($p < 0.002$, one-way ANOVA, post hoc Tukey multiple comparisons test, $n = 9$) (Fig. 1B). The percentage of T62D-hDAT delivered to the plasma membrane was not altered because the total expression of the mutant was also decreased in comparison with hDAT or T62A-hDAT (biotinylated/total: hDAT, 0.73 ± 0.05; T62A-hDAT, 0.77 ± 0.1; T62D-hDAT, 0.55 ± 0.08; $p = 0.1$, one-way ANOVA, $n = 9$).

The velocity of [^{3}H]DA uptake for these mutants was determined by measuring the initial rate of uptake calculated from time course curves for varying concentrations of [^{3}H]DA. The calculated V_{max} value for T62D-hDAT was significantly lower than that of hDAT (0.82 ± 0.17 pmol/min/10^5 cells for hDAT, $n = 6$, and 0.04 ± 0.005 pmol/min/10^5 cells for T62D-hDAT, $n = 6$). After normalization of the data to the expression of hDAT, the V_{max} value for T62D-hDAT is 0.07 ± 0.01 pmol/min, as shown in Fig. 2. The V_{max} value for T62A-hDAT, which had the same surface expression as hDAT, is 0.38 ± 0.03 pmol/min/10^5 cells, $n = 5$. The V_{max} value for [^{3}H]DA uptake by both T62D-hDAT and T62A-hDAT differs significantly from those of hDAT (one-way ANOVA, $p = 0.0004$; in post hoc Bonferroni testing, hDAT differs from T62D-hDAT at $p < 0.001$ and from T62A-hDAT at $p < 0.05$). Likewise, the K_m values for DA are significantly different for T62D-hDAT (0.16 ± 0.1 μM) and T62A-hDAT (0.82 ± 0.1 μM) compared with hDAT (2.1 ± 0.3 μM) (ANOVA, $p = 0.0003$; in Bonferroni post hoc testing, hDAT differs from T62A at $p < 0.01$ and from T62D-hDAT at $p < 0.001$). The turnover numbers, or k_{cat}, are 0.2/s, 0.07/s, and 0.02/s for the hDAT, T62A-hDAT, and T62D-hDAT, respectively. However, the k_{cat}/K_m value, a second-order rate constant

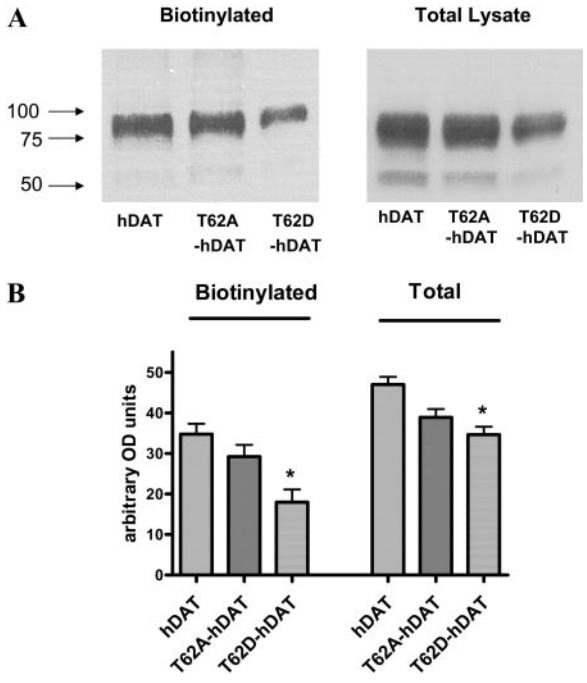

Fig. 1. Surface expression of hDAT and mutant hDAT in HEK 293T cells. A, cell surface expression of hDAT and mutant hDAT proteins was measured by biotinylation of cell surface proteins with sulfo-NHS-SS-biotin as described under *Materials and Methods*. Biotinylated proteins were isolated using avidin beads and analyzed by Western blotting using a monoclonal anti-DAT antibody. The position of the 100-, 75-, and 50-kDa molecular mass markers is shown. B, quantitation of the biotinylated surface and total (in lysate) hDAT proteins in hDAT and mutant hDAT cells. The expression of the constructs was measured by Scion Image software. Mean arbitrary density units were plotted ($n = 6$) for the surface hDATs (biotinylated) and total hDAT (lysate) for the hDAT, T62A-, and T62D-hDAT constructs. *, one-way ANOVA, $p < 0.002$; in post-hoc Tukey-Kramer analysis, $p < 0.01$ for hDAT versus T62D-hDAT, $p < 0.05$ for T62A-hDAT versus T62D-hDAT. For lysate totals, one-way ANOVA, $p < 0.001$; in post-hoc Tukey-Kramer analysis, $p < 0.001$ for hDAT versus T62D-hDAT; $p < 0.05$ for T62A-hDAT versus T62D-hDAT.

of the association of DA with the transporter, for hDAT and T62A-hDAT does not differ, and the value of k_{cat}/K_m for [^{3}H]DA uptake through T62D-hDAT is only 25 to 30% less than for the other two constructs. The k_{cat}/K_m values for the hDAT, T62A-hDAT, and T62D- hDAT mutants are 9.3×10^4, 8.6×10^4, and 5.0×10^4 $s^{-1} \cdot M^{-1}$, respectively.

Basal Efflux of DA in hDAT and the Thr62 Mutants. Curiously, although the k_{cat}/K_m for T62D-hDAT in the initial rate experiments was not dramatically impaired, we observed extremely low accumulation of DA over time. One possible explanation for this reduction is that basal DA efflux could be elevated in T62D-hDAT, resulting in reduced accumulation of intracellular DA. To assess this possibility, cells were preloaded with 5 μM [^{3}H]DA for 20 min at room temperature. This incubation with 5 μM [^{3}H]DA did not change surface DAT for any of the three mutants (data not shown). The cells were rapidly washed, and the buffer was removed and replaced at 10-min intervals, as described under *Materials and Methods*. In Fig. 3, [^{3}H]DA efflux is expressed as a percentage of the total amount of [^{3}H]DA measured in the cells before the collection period (basal fractional efflux). Whereas basal fractional efflux in hDAT and T62A-hDAT cells is relatively low, in T62D-hDAT cells, it is significantly higher at each time point and highest at the earliest time point measured (10 min). The total DA content in the hDAT, T62A-hDAT, and T62D-hDAT cells at the end of the loading period was 32.6 ± 7, 23 ± 7 and 1.1 ± 0.1 pmol DA/10^5 cells (n = 8), respectively. These results suggest that T62D-hDAT is unable to concentrate intracellular DA in response to high extracellular DA because of a high basal efflux.

To test whether DA uptake by T62D-hDAT is overcome by basal DA efflux, we measured basal DA efflux in a single cell by amperometry after loading the cell with 1 μM DA for 45 min at 37°C. Figure 4 shows representative amperometric traces for hDAT (Fig. 4A), T62A-hDAT (Fig. 4B). and T62D-hDAT (Fig. 4C) under control conditions and after bath application of cocaine (arrow). The data in Fig. 4D show the DAT-mediated cocaine-sensitive current that is the difference between the current recorded under control conditions and the current recorded in the presence of cocaine. These data demonstrate the presence of a significantly greater basal DA leak in T62D-hDAT compared with hDAT and T62A-hDAT. Furthermore, the difference is probably greater than shown because the levels of surface DAT in T62D-hDAT is approximately half that of hDAT and T62A-hDAT.

The results shown in Figs. 3 and 4 suggest that T62D-hDAT has a greater facility to elicit efflux than either hDAT or T62A-hDAT. To assess the catalytic effectiveness of the T62D-hDAT, we measured the kinetic constants for the outward transport of [^{3}H]DA through the mutant and compared them with the values for hDAT. T62D-hDAT and hDAT cells were incubated with concentrations of [^{3}H]DA from 1 to 80 μM for 30 min at room temperature. After the incubation, the cells were rapidly washed three times with KRH, and basal efflux of [^{3}H]DA was measured at 10-s intervals from 0 to 30 s. The intracellular [^{3}H]DA concentration was calculated by considering the volume of an HEK 293 cell to be approximately 1.25 pl (Sitte et al., 2001). Using initial rate values for efflux, and the initial concentration of [^{3}H]DA calculated using the initial [^{3}H]DA content and cell volumes, Michaelis-Menten curves for [^{3}H]DA efflux through the two DAT mutants were constructed (Fig. 5). Analysis of the absolute sum of squares residuals using Prism 5 demonstrated that these lines better fit a Michaelis-Menten hyperbola than a straight line. The V_{max} values for the outward flow of [^{3}H]DA through T62D-hDAT and hDAT in pmol/10^5 cells/min are 14.5 ± 1 and 7.2 ± 0.5, respectively. The normalized value for T62D-hDAT compared with surface hDAT was 15.1 pmol/min, and the normalized values are shown in Fig. 5. However, the K_m value for efflux of [^{3}H]DA is significantly reduced in the T62D-hDAT mutant compared with hDAT (629 versus 42 μM for hDAT and T62D-hDAT, respectively; $p < 0.0001$, $F_{1,34} = 25.42$). From these values, we calculated the turnover numbers for outward transport at 25°C for the two mutants, which were 3.3/s for hDAT and 3.2/s for T62D-hDAT. Although the turnover numbers are equivalent for hDAT and T62D-hDAT, the second-order rate constant of association of DA with the transporter (k_{cat}/K_m) is 14.6 times greater for

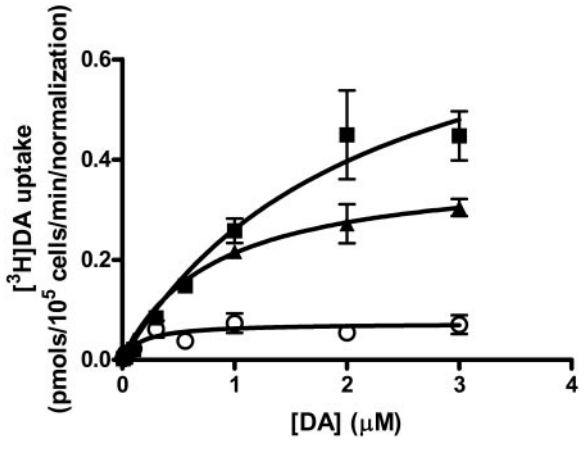

Fig. 2. Uptake kinetics of [^{3}H]DA in cells expressing hDAT and mutant hDAT. [^{3}H]DA uptake was measured at indicated DA concentrations under initial rate conditions as described under *Materials and Methods* in hDAT(■), T62A-hDAT (▲), and T62D-hDAT (○) cells. Kinetic analysis was performed by nonlinear regression analysis of the individual experiments for each mutant using GraphPad Prism version 4.

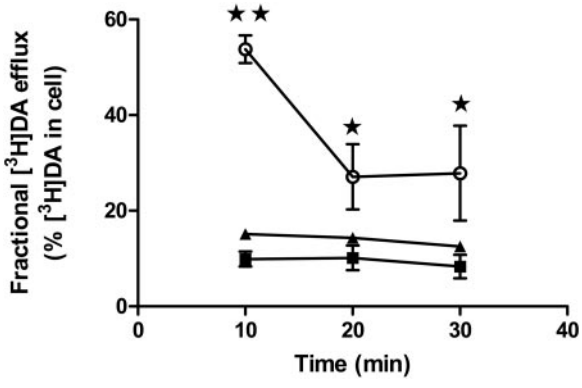

Fig. 3. Enhanced basal DA efflux in T62D-hDAT cells. Cells were preincubated with 5 μM [^{3}H]DA in KRH for 20 min at room temperature, and basal efflux was measured in hDAT (■), T62A-hDAT (▲), and T62D-hDAT (○) cells as described under *Materials and Methods*. Efflux measured at various times is calculated as the percentage of total [^{3}H]DA in the cell at the start of the experiment (n = 8). The total DA content in the hDAT, T62A-hDAT, and T62D-hDAT cells at the end of the loading period was 32.6 ± 7, 23 ± 7, and 1.1 ± 0.1 pmol DA/10^5 cells (n = 8). Analysis of the data by two-way ANOVA demonstrates a significant interaction of the different mutants and time ($p = 0.0026$), as well as differences among the mutants ($p < 0.001$) and time ($p < 0.001$). In Bonferroni post tests, **, $p < 0.001$, compared with hDAT and T62A-hDAT; *, $p < 0.05$ compared with hDAT and T62A-hDAT.

T62D-hDAT (7.7×10^4 $s^{-1} \cdot M^{-1}$) than that for hDAT (0.053×10^5 $s^{-1} \cdot M^{-1}$) due to the lower K_m value for T62D-hDAT.

Zn^{2+} Rescues T62D-hDAT-Mediated DA Uptake. The increased basal efflux in T62D-hDAT could be due to a conformational change that increases the partitioning of the transporter in the membrane toward inward-facing conformation. To test this hypothesis, we used the demonstrated ability of Zn^{2+} to partially "rescue" the conformational state of DAT mutants that are predominantly inward-facing (Loland et al., 2002, 2004). Occupancy of the endogenous Zn^{2+} binding site in hDAT (His193, His375, and Glu396) has been suggested to favor an outward-facing conformation and, to a large extent, inhibit DA uptake (Norregaard et al., 1998; Loland et al., 1999). We reasoned that the addition of Zn^{2+} to T62D-hDAT should diminish the preference for the inward-facing conformation and enhance substrate uptake. Consistent with this hypothesis, in the presence of Zn^{2+}, [^{3}H]DA uptake is significantly increased in T62D-hDAT cells compared with hDAT (Fig. 6). As expected, increasing concentrations of Zn^{2+} reduce [^{3}H]DA uptake in hDAT cells. It is noteworthy that the sensitivity of T62A-hDAT to the inhibition of [^{3}H]DA uptake by Zn^{2+} is greatly increased (Fig. 6), although the extent of inhibition is comparable with hDAT. Thus, [^{3}H]DA uptake into T62A-hDAT cells is significantly inhibited by 10 nM and 30 nM Zn^{2+} concentrations, which have no effect on [^{3}H]DA uptake into hDAT cells. This is consistent with the data showing that T62A-hDAT differs from the wild type but does not have as extreme a phenotype as T62D-hDAT.

Characterization of AMPH-Stimulated DA Efflux in hDAT and the Thr62 Mutants. We have demonstrated previously that influx and efflux of DA can be independently regulated by mutations in hDAT (Khoshbouei et al., 2004). Because of the high baseline efflux, we predicted that T62D-hDAT might not be responsive to AMPH, but the T62A-hDAT mutant may respond to AMPH in a manner different from hDAT. The hDAT, T62A-hDAT, and T62D-hDAT cells were preincubated with [^{3}H]DA for 20 min, and [^{3}H]DA efflux in response to AMPH was measured. Because the amount of [^{3}H]DA present in the cells during the 20-min incubation differed among the mutants (Fig. 7), AMPH-stimulated [^{3}H]DA efflux was calculated as fractional release, which is the percentage of [^{3}H]DA in the eluate compared with the total cellular [^{3}H]DA before the addition of AMPH. As shown in Fig. 7A, a reduction in AMPH-stimulated DA efflux was apparent in T62A-hDAT cells compared with hDAT cells. V_{max} values for efflux (expressed as the fractional release of [^{3}H]DA per 5 min) were 7.7 and 3.9 ($p < 0.005$, $F_{1,81} = 8.322$, $n = 8$), and the K_m values for AMPH were 1.3 and 0.7 μM for hDAT and T62A-hDAT, respectively (not significant). Therefore, the T62A mutant was compromised in both inward and outward transport.

As expected, we were unable to detect AMPH-stimulated [^{3}H]DA efflux from T62D-hDAT cells (Fig. 7A), although low levels of cytoplasmic DA could be detected in the cells after loading with 5 μM [^{3}H]DA. If the T62D-hDAT mutant is constitutively transporting DA outward, a lack of effect of AMPH would be expected. However, the inability of AMPH to cause DA efflux could also result from an impaired interaction of AMPH with this mutant. To assess this possibility, we examined the ability of AMPH to block the uptake of 30 nM [^{3}H]DA in the mutant cells. As shown in Fig. 7B, T62D-hDAT cells had a higher affinity for AMPH than either T62A-hDAT or hDAT cells. The IC_{50} values for the hDAT, T62A-, and T62D-hDAT mutants were 1600, 657 and 104 nM, respectively ($p < 0.0002$, $F_{2,45} = 10.6$, $n = 3$). The IC_{50} value for AMPH in T62A-hDAT cells did not significantly differ from that in hDAT cells.

Thus, our data are consistent with the hypothesis that the constitutive efflux of DA through T62D-hDAT precludes regulation by AMPH. To circumvent the problem of constitutive efflux, the T62D-hDAT cells were loaded with DA in the presence of Zn^{2+}, which permits the accumulation of DA. In these experiments, cells were loaded with 5 μM unlabeled DA for 30 min at 37°C, in the presence and absence of 30 μM Zn^{2+}, perfused with buffer and AMPH, and DA was measured by high-performance liquid chromatography with electrochemical detection. We predicted that preloading and superfusion of T62D-hDAT cells in the presence of Zn^{2+} would reduce basal efflux and restore AMPH-stimulated efflux. Incubation with Zn^{2+} permitted the accumulation of intracellular DA to levels comparable with those of hDAT T62D-hDAT without Zn^{2+}, 3.8 ± 0.9 nmol/mg protein; T62D-hDAT

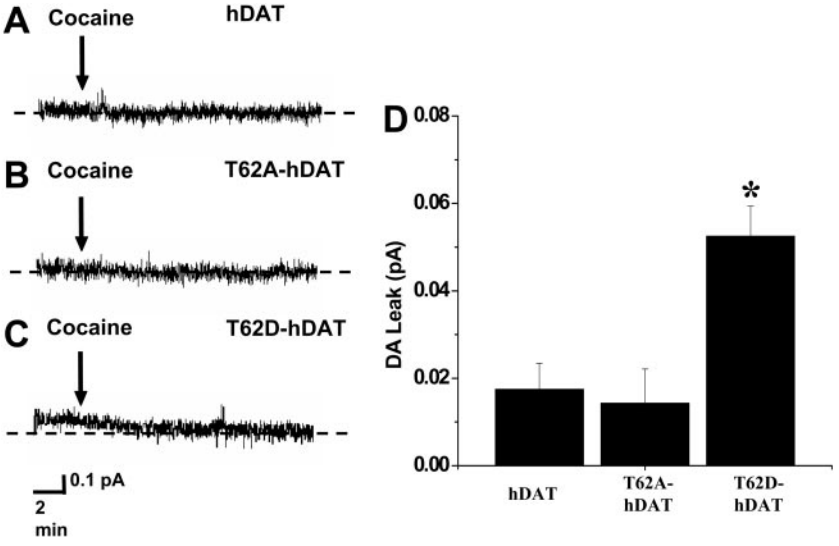

Fig. 4. T62D mutation confers DA leak. Representative amperometric current obtained from hDAT (A), T62A-hDAT (B), and T62D-hDAT (C). Cells were preloaded by incubating them in a bath solution containing 1 μM DA. Cells were then washed, and DA leak was estimated by measuring the decrease in amperometric current upon cocaine application. D, DA leak from hDAT ($n = 8$), T62A-hDAT ($n = 7$), and T62D-hDAT ($n = 12$) cells reported as mean ± S.E.M. The dotted horizontal lines represent the amperometric currents recorded when all dopamine transporters are blocked by cocaine. *, one-way ANOVA, $p < 0.001$; in Bonferroni post tests, $p < 0.01$ for T62D-hDAT versus T62A-hDAT and hDAT.

with Zn^{2+}, 12.2 ± 1.6 nmol/mg protein; hDAT without Zn^{2+}, 10.5 ± 0.3 nmol/mg protein; hDAT with Zn^{2+} 11.8 ± 0.6 nmol/mg protein). As shown in Fig. 8, AMPH stimulates DA efflux in T62D-hDAT to levels equivalent to those of hDAT when Zn^{2+} is present both during the DA loading and during AMPH exposure. In hDAT, a concentration of Zn^{2+} that inhibits DA uptake promotes AMPH-stimulated efflux, as observed previously by others (Scholze et al., 2002). Indeed, it has been suggested that the ability of Zn^{2+} to stabilize the transporter in an outward-facing state facilitates transporter reversal (Scholze et al., 2002).

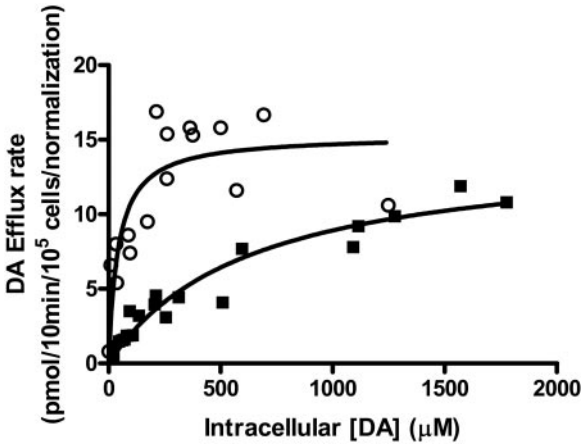

Fig. 5. Kinetic analysis of [^{3}H]DA efflux in hDAT and T62D-hDAT. hDAT (■) or T62D-hDAT (○) cells (1×10^5) were preloaded by incubating them in KRH containing 60 or 120 nM [^{3}H] DA and varying concentrations of unlabeled DA (1–80 μM) for 30 min at 25°C. After loading, the efflux experiment was conducted at 25°C. Cells were washed rapidly with KRH, and fresh buffer was added. Specific efflux was determined in the presence and absence of 100 μM cocaine. The intracellular concentrations of DA were calculated in micromoles using 1.25 pl as the volume of an HEK 293 cell (Sitte et al., 2001). Initial rates of efflux were determined from 0 to 30 s (every 10 s) and plotted against the intracellular concentration of [^{3}H]DA. V_{max} and K_m values for efflux were calculated using nonlinear regression analysis in Prism 4. Statistical significance was determined with an F test using Prism version 4. The null hypothesis was that the best-fit parameter for the value did not differ among the two cell types. A conclusion of statistical significance represents a rejection of the null hypothesis and indicates a difference among designated values. K_m values for the two mutants differed at $p < 0.0001$.

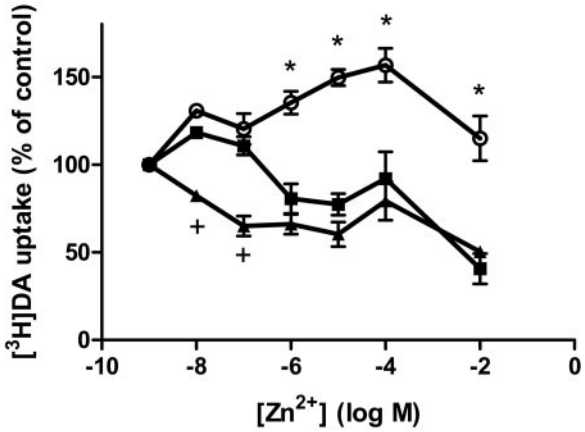

Fig. 6. Zn^{2+} potentiates DA uptake in T62D-hDAT. The hDAT (■), T62A-hDAT (▲), and T62D-hDAT (○) cells were incubated with 15 nM [^{3}H]DA, and indicated concentrations of Zn^{2+} and [^{3}H]DA uptake were measured as explained under *Materials and Methods*. Values are the percentage of control of [^{3}H]DA uptake in cells in the absence of Zn^{2+} (n = 3). In two-way ANOVA analysis, $p < 0.0001$ for Zn^{2+}, mutants, and the interaction. In post hoc Bonferroni testing, *, $p < 0.001$ for hDAT versus T62D-hDAT and T62A-hDAT; +, $p < 0.01$ for hDAT versus T62A-hDAT. All points for T62D-hDAT differed from those for T62A-hDAT at $p < 0.001$. The counts per minute for [^{3}H]DA taken up in the absence of Zn^{2+} were 4486 ± 320 (hDAT), 1770 ± 251 (T62A-hDAT), and 1528 ± 87 (T62D-hDAT).

To measure efflux in T62D-hDAT cells without the confounding effects of DA loading and/or Zn^{2+} treatment, T62D-hDAT cells were voltage-clamped in the whole-cell configuration, whereas DA efflux was simultaneously monitored by amperometry. The whole-cell patch pipette was filled with an internal solution containing 30 mM NaCl and 2 mM DA, which is sufficient to sustain DA efflux (Khoshbouei et al., 2003). The DAT-mediated amperometric currents (DA efflux) are defined by subtracting the current recorded in the presence of cocaine from the current recorded in vehicle-treated control. The data of Fig. 9A show that under voltage-clamped conditions, T62D-hDAT cells exhibit DA efflux, and at positive voltages, the efflux does not differ from that of hDAT. However, it is noteworthy that, at −20 mV, which resembles

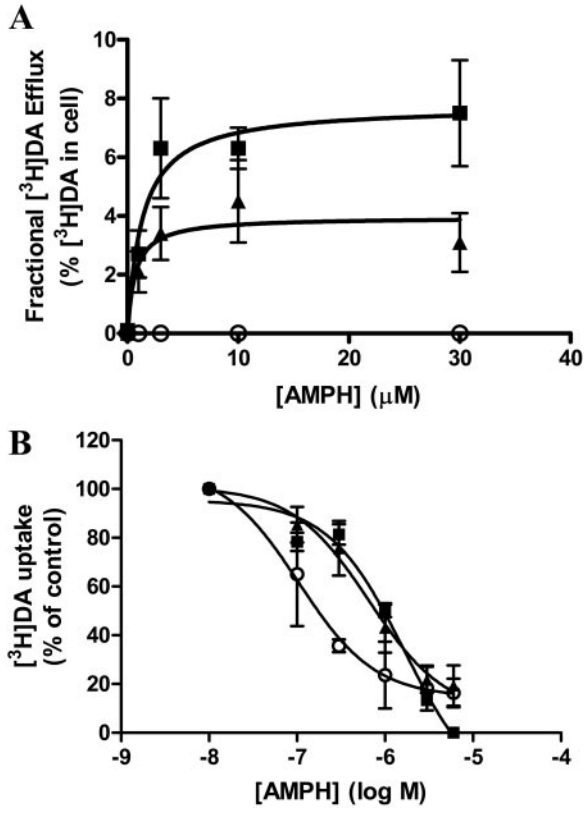

Fig. 7. AMPH-induced DA efflux in hDAT and the T62A-hDAT cells. A, cells (100,000/well) were incubated with 5 μM DA containing 30 nM [^{3}H]DA for 20 min, washed, and treated with indicated concentrations of AMPH as described under *Materials and Methods*. AMPH-mediated DA efflux is expressed as the fractional release of cellular [^{3}H]DA per 5 min, in hDAT (■), T62A- (▲), and T62D- (○) hDAT cells. Statistical analysis was performed with an F test using Prism version 4 as described in Fig. 2. Total initial [^{3}H]DA in the cells was 32 ± 7 pmol/10^5 cells for hDAT, 23 ± 6 pmol/10^5 cells for T62A-hDAT, and 1.1 ± 0.1 pmol/10^5 cells for T62D-hDAT, n = 8. The V_{max} for AMPH-stimulated [^{3}H]DA efflux was 7.8 pmol/5 min/10^5 cells in hDAT cells and 3.9 pmol/5 min/10^5 cells in T62A-hDAT cells (p = 0.002, $F_{2,86}$ = 6.561, n = 6–10). There was no significant difference in K_m values for AMPH between hDAT cells (1.3 μM) and T62A-hDAT cells (0.7 μM). There was no [^{3}H]DA efflux in response to AMPH in T62D-hDAT cells. B, DA uptake in hDAT(■), T62A-hDAT (▲), and T62D-hDAT (○) cells in the presence of increasing concentrations of AMPH. Cells were incubated with 30 nM [^{3}H]DA for 10 min at room temperature and processed as described under *Materials and Methods*.

the resting membrane potential of HEK 293 cells, T62D-hDAT exhibited significantly greater DA efflux compared with T62A-hDAT and hDAT (one-way ANOVA, $p \leq 0.01$), indicating that the T62D mutation confers the ability to efflux at negative resting membrane potentials. The differences between T62D-hDAT and hDAT are probably greater than shown in Fig. 9A, however, because the levels of surface DAT for T62D-hDAT are approximately half that of hDAT. Therefore, the values for T62D-hDAT are an underestimate of the true values. At depolarizing membrane potentials, DA efflux mediated by T62A-hDAT was significantly less than that of hDAT or T62D-hDAT (two-way ANOVA, $p < 0.0001$ for voltage, $p < 0.001$ for mutant and $p < 0.001$ for interaction; in post hoc Bonferroni testing, efflux through T62A-hDAT differed from both hDAT and T62D-hDAT as indicated in Fig. 9A).

A good correlation between the ability of substrates to induce currents and their ability to cause efflux has been reported previously (Sitte et al., 1998). However, the elicited whole-cell currents through DAT exceed the predicted stoichiometry (Sitte et al., 1998). We found the whole-cell currents measured through T62D-hDAT to be significantly greater at positive voltages than those carried through hDAT or T62A-hDAT cells (Fig. 9B). When analyzed by two-way ANOVA, the curves differed for mutant ($p < 0.001$) and voltage ($p < 0.001$) but not for the interaction. In post hoc Bonferroni testing, the whole-cell currents for T62D-hDAT and T62A-hDAT differed at 60 mV ($p < 0.05$). Unlike the amperometric currents, the whole-cell currents for T62A-hDAT were not significantly different from hDAT. It is noteworthy that the apparent reversal potential of the hDAT-mediated current was not affected by mutation of Thr62, suggesting that these mutations do not affect the ionic gradient across the plasma membrane.

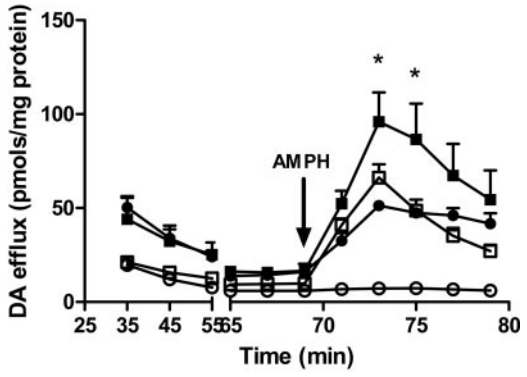

Fig. 8. AMPH stimulated DA efflux in hDAT- and T62D-hDAT cells in the presence and absence of Zn^{2+}. T62D-hDAT cells were loaded with 5 μM DA as described under *Materials and Methods* in the presence of 30 μM Zn^{2+}, and hDAT cells were loaded in the absence of Zn^{2+} at 37°C for 30 min. AMPH-stimulated DA efflux was measured by superfusion as described under *Materials and Methods* in either the presence (■, hDAT; ●, T62D-hDAT) or absence of Zn^{2+} (□, hDAT; ○, T62D-hDAT) of 30 μM Zn^{2+} as indicated ($n = 3$). Baseline values of [^{3}H]DA were collected for 70 min until the addition of 10 μM AMPH (arrow). Initial levels of DA in the cells were the following: T62D-hDAT without Zn^{2+}, 3.8 ± 0.9 nmol/mg protein; T62D-hDAT with Zn^{2+}, 12.2 ± 1.6 nmol/mg protein; hDAT without Zn^{2+}, 10.5 ± 0.3 nmol/mg protein; hDAT with Zn^{2+}, 11.8 ± 0.6 nmol/mg protein. In two-way ANOVA analysis, $p < 0.0001$ for time (fraction) and the mutant/Zn^{2+} condition; $p < 0.0001$ for the interaction; *, $p < 0.01$ for hDAT with Zn^{2+} versus all other groups. T62D-hDAT with no Zn^{2+} differed from all other groups at $p < 0.001$. There was no statistical difference between hDAT with no Zn^{2+} and T62D-hDAT with Zn^{2+}.

Discussion

We show that Thr62 in the juxtamembrane N-terminal domain of the human DAT plays a critical role in transporter function. Analysis of a somewhat conservative and a nonconservative substitution at this site reveals differential effects. Both substitutions alter function, with a more drastic effect caused by the nonconservative substitution (threonine to aspartate). The functional significance of Thr62 is underscored by the fact that the motif containing Thr62 (RETW) is highly conserved in all monoamine transporters (Vaughan, 2004), and the RXXW sequence is fully conserved throughout the family of sodium/chloride-dependent neurotransmitter transporters. In addition, RETW is a canonical phosphorylation site for PKC/cGPK/PKA, suggesting that the threonine might be phosphorylated. The crystal structure of $LeuT_{Aa}$, a bacterial homolog of the sodium/chloride-dependent transporter, suggests that this sequence is part of a conserved network of cytoplasmic interactions that may be critical in forming the intracellular gate (Yamashita et al., 2005), although threonine in this motif is not in LeuT. The addition of a negative charge (as in aspartate or phosphothreonine) to the RETW motif could have a profound effect on the movement of this

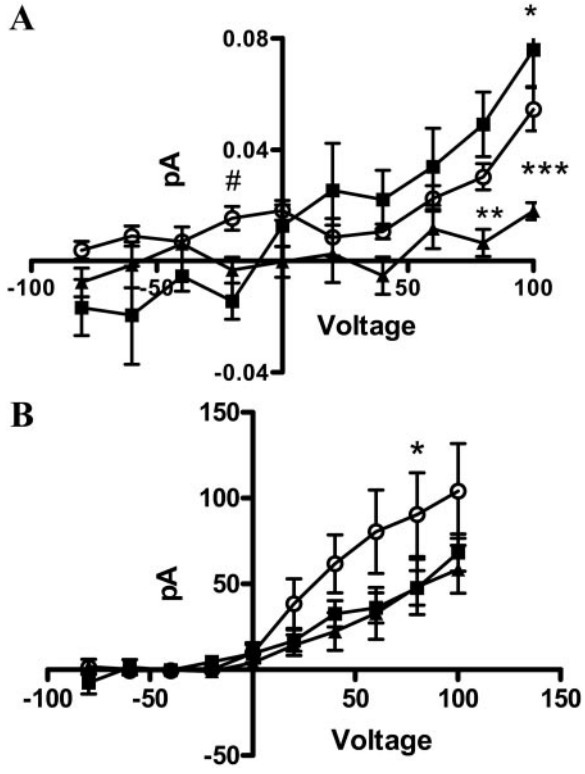

Fig. 9. Current-voltage and amperometric-voltage relationships from hDAT, T62A-, and T62D-hDAT cells. Amperometric-voltage relationship (A) and current-voltage relationship (B) obtained from hDAT (■), T62A-hDAT (▲), and T62D-hDAT (○) in the presence of 30 mM Na^+ in cells loaded with 2 mM DA, whereas the membrane potential was stepped from a holding potential of −20 mV to voltages between −100 to +100 in 20-mV increments (means ± S.E.M., $n = 6$). A, in a two-way ANOVA, $p < 0.001$ for mutant, for voltage and interaction. In post hoc Bonferroni testing, **, $p < 0.01$; ***, $p < 0.001$ for T62A-hDAT compared with hDAT; *, $p < 0.05$ for T62D-hDAT compared with hDAT. In a one-way ANOVA comparing values at −20 mV, #, $p = 0.0037$ for T62A-hDAT compared with T62D-hDAT. B, in two-way ANOVA, $p < 0.001$ for mutant and for voltage. In post hoc Bonferroni testing, *, $p < 0.05$ for T62D-hDAT compared with T62A-hDAT.

intracellular gate in monoamine transporters, as discussed below.

Our results indicate that mutation of Thr62 to aspartate alters the conformational equilibrium of the DAT transport cycle such that the free transporter partitions predominantly in inward-facing conformation, which can readily mediate constitutive DA efflux. This inference is suggested by the significant reduction in [^{3}H]DA uptake into T62D-hDAT cells versus hDAT, as would be expected if the mutant construct favored an inward-facing conformation. Data in the literature support such an inference, because mutations postulated to arrest the transporter in inward-facing conformations consistently exhibit a reduced V_{max} value of DA uptake (Loland et al., 2002, 2004; Chen et al., 2004; Korkhov et al., 2006). Strikingly, the affinity for uptake of two substrates, DA and AMPH, was increased in the T62D-hDAT mutant compared with hDAT. Increased sensitivity to substrates was reported in D345N-hDAT (Chen et al., 2004), which seemed to be predominantly inward-facing as a result of an inability to reorient to the extracellular side. Impairment of the return of an empty transporter from inward- to outward-facing state would reduce both V_{max} and K_m values. Because both V_{max} and K_m values for T62D-hDAT were reduced compared with hDAT, the overall catalytic effectiveness of the uptake process in T62D-hDAT was only 30% less than in hDAT. The second-order rate constant (V_{max}/k_{cat}), however, is much lower than that reported in another study using hDAT-HEK cells ($1.2 \times 10^7\ M^{-1} \cdot s^{-1}$) (Earles and Schenk, 1999). Lower temperature (25 versus 37°C) could partially account for this, but other factors could be our construct or the cells.

Strikingly, efflux of intracellular substrate in T62D-hDAT was increased in the absence of stimulation with either AMPH or voltage. In hDAT, the catalytic effectiveness of uptake was greater than that for efflux, largely because the K_m value for DA efflux is ~40 times greater than for DA influx. The decrease in the K_m value for DA at the inward-facing side of T62D-hDAT compared with hDAT could explain the constitutive efflux through this mutant. As might be expected for a transporter in a predominantly inward-facing state, AMPH was ineffective in stimulating efflux. A major role of AMPH influx is to move Na^+ through the transporter and increase the availability of Na^+ at the inner face of the transporter (Rutledge, 1978; Khoshbouei et al., 2003); this requirement could be precluded in a transporter that is predominantly inward-facing.

Binding of Zn^{2+} to the endogenous Zn^{2+} binding site in DAT stabilizes the outward-facing conformation and facilitates reorientation of the inward-facing transporter (Loland et al., 2002). The T62D mutation converted the inhibitory effect of Zn^{2+} on DA uptake to a stimulatory effect, consistent with a shift away from an outward-facing conformation. Accordingly, in T62D-hDAT, Zn^{2+} increases DA uptake and permits wild-type AMPH-stimulated DA efflux. Our experiments using amperometry, in which DA is added intracellularly, strongly support a shift of T62D-hDAT toward an inward-facing conformation. Not only was an enhanced "leak" of DA measured by amperometry from the T62D-hDAT mutant, but DA efflux was observed at negative potentials from T62D-hDAT, as opposed to hDAT or T62A-hDAT. Finally, the increased current through T62D-hDAT compared with T62A-hDAT in the current-voltage relationship supports the hypothesis of an efflux-preferring conformation because there is a positive correlation between transporter-mediated currents and efflux through the transporter (Sitte et al., 1998). However, the apparent ion flux through the three transporter constructs was not different because the reversal potential was the same for all three.

The fact that the initial rate of influx through T62D-hDAT was severely reduced but not abrogated demonstrates that T62D-hDAT can transition to the outward-facing conformation and does not have a defect in reorientation of the transporter as observed in D345N-hDAT (Chen et al., 2004) and E136A-human serotonin transporter (Korkhov et al., 2006). The Thr62 to alanine substitution generates a transporter with properties that differ from hDAT but are less severe, demonstrating a reduction in DA uptake and AMPH-stimulated efflux. Reduced [^{3}H]DA uptake compared with rDAT

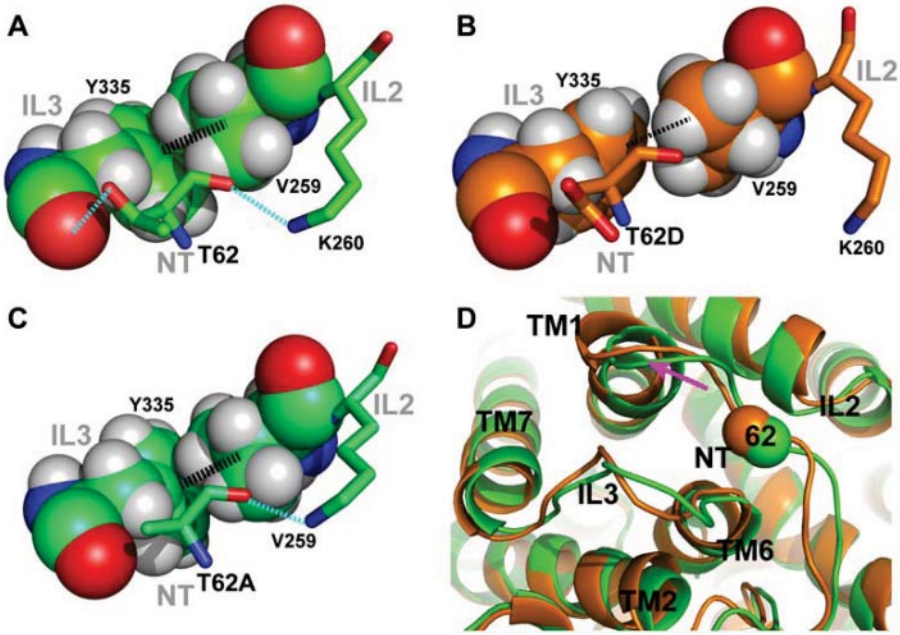

Fig. 10. Molecular modeling of hDAT and its in silico mutagenesis. In our three-dimensional hDAT model, Thr62 is located at the junction of the N terminus (NT), the intracellular loop 2 (IL2), and IL3, which constitutes a critical portion of the intracellular interaction network. Specifically, the side chain of Thr62 (A) forms a hydrogen bond with the backbone carbonyl of Tyr335 of IL3 (dotted line in cyan); the backbone of Thr62 interacts with Lys260 of IL2 (dotted line in cyan), whereas the adjacent residue Val259 is closely packed with the phenol ring of Tyr335 (dotted thick line in black). In T62D mutation (see *Materials and Methods* for the in silico mutagenesis procedure), both of the "cyan" interactions are lost, presumably due the repulsion between the carboxyl group of aspartate and the backbone carbonyl of Tyr335; the hydrophobic-aromatic interaction of Val259-Tyr335 is also significantly weakened (B). In the T62A mutant, the interaction between position 62 and Tyr335 is lost, but the other two interactions are nevertheless largely maintained (C). D, the impact of T62D (orange) on local conformation, compared with hDAT (green), with the Cα atoms of residue 62 in sphere representation. Within the time scale of our simulations of the T62D mutant, the cytoplasmic end of TM1 moves away from TM6–IL3 and IL2.

was demonstrated in T62A-rDAT cells (Lin et al., 2003). The reduction in DA efflux through T62A-hDAT is more extreme when efflux is measured by amperometry (Fig. 9A) than by [^{3}H]DA efflux (Fig. 7). Amperometry measurements, however, are performed on a millisecond time scale in voltage-clamped cells as opposed to the longer incubation method, suggesting that the Thr62 to alanine mutation may slow the equilibrium between inward- and outward-facing states. The greater sensitivity to inhibition by Zn^{2+} could also be explained by a reduced capacity for T62A-hDAT to transition between inward and outward states. The similar degree of reduction (~50% of hDAT) of both influx and efflux of DA in T62A-hDAT suggests that both inward-outward and outward-inward equilibria are slowed.

In view of the remarkable conservation of threonine at this position, it is important to understand the differential impact of T62A and T62D on the pharmacological properties of hDAT from the structural perspective. Using the molecular model of the transporter, we conducted MD and FEP studies to characterize the effects of the mutations at the molecular level. First, MD simulation was used to reveal the local conformational divergence from the LeuT structure (Yamashita et al., 2005) because of the presence of a threonine at position 62 in the DAT model. The -OH group of Thr62 engages in important interactions, as evidenced by the consistency along the 16-ns MD trajectory of the hydrogen bond with the backbone carbonyl group of Tyr335 from IL3, whereas the Thr62 backbone interacts with the side-chain of Lys260 from IL2. In this local region, similar to the observation in the LeuT crystal structure, the cation-π interaction between Tyr335 and Arg60 is stabilized by the aromatic-hydrophobic interaction of Tyr335 with Val259 (Fig. 10A). This network of interactions is modified in the mutant in a manner described by the in silico mutations that we introduced with the FEP procedure (see *Materials and Methods*). We found that the T62D mutation is associated with a loss of both interactions, with Tyr335 and Lys260, and that the interactions between Tyr335 and Val259 is weakened (Fig. 10B). The orientation of Tyr335 toward Arg60 is affected accordingly (data not shown), generating a significant conformational change in which the cytoplasmic end of TM1 moves away from the junction point with IL2 and IL3 (Fig. 10D, shown with a pink arrow). In the T62A mutant, only the interaction with Tyr335 is lost, whereas the other interactions in this local network mentioned above are largely maintained (Fig. 10C). Thus, dramatic changes are produced in the structure of a functionally important microenvironment after the mutation of Thr62 to aspartate, which demonstrates the critical role of this residue in facilitating the interactions between IL2 and IL3, which are probably involved in the transition between the inward-facing and outward-facing conformations.

There is evidence for phosphothreonine in DAT (Foster et al., 2002). Thr62, contained within a consensus sequence for PKC/cGPK/PKA (RETW), could be phosphorylated in vivo. It is noteworthy that Thr276 in IL2 of the serotonin transporter is directly adjacent to the network of interactions identified here. This residue is phosphorylated by cGPK (Ramamoorthy et al., 2007), consistent with the possibility that Thr62 may be phosphorylated as well. The altered conformation of DAT as a result of Thr62 mutation could affect function by altering the binding of other proteins to DAT, such as syntaxin and receptor for activated C kinase 1. A T62A mutation of rDAT rendered it almost completely insensitive to the effect of phosphatidylinositol 3 kinase inhibition and mitigated the effect of protein kinase C activation on DA uptake (Lin et al., 2003).

In conclusion, our data identify mechanisms involving Thr62 as a residue important for DAT function. A nonconservative substitution at this residue, (as in threonine to aspartate) seems to shift the conformation of DAT from the physiologically favored substrate influx mode to an efflux promoting one—a conformational switch promoted by drugs of abuse, such as AMPH, which are also DAT substrates. Mutating Thr62 to alanine seems to produce a transporter that is slower to transition between inward- and outward-facing conformations. Because Thr62 is a highly conserved residue in monoamine transporters, its role in regulating hDAT function is likely to be replicated in other monoamine transporters as well.

Acknowledgments

We thank Susana Shamban, Charles Lo, Hobart Ng Ng Tsai, and Christina Chi for technical assistance.

References

Beuming T, Shi L, Javitch JA, and Weinstein H (2006) A comprehensive structure-based alignment of prokaryotic and eukaryotic neurotransmitter/Na^+ symporters (NSS) aids in the use of the LeuT structure to probe NSS structure and function. *Mol Pharmacol* **70:**1630–1642.

Chen N and Justice JB (2000) Differential effect of structural modification of human dopamine transporter on the inward and outward transport of dopamine. *Brain Res Mol Brain Res* **75:**208–215.

Chen N and Reith ME (2000) Structure and function of the dopamine transporter. *Eur J Pharmacol* **405:**329–339.

Chen N, Rickey J, Berfield JL, and Reith ME (2004) Aspartate 345 of the dopamine transporter is critical for conformational changes in substrate translocation and cocaine binding. *J Biol Chem* **279:**5508–5519.

Earles C and Schenk JO (1999) Multisubstrate mechanism for the inward transport of dopamine by the human dopamine transporter expressed in HEK cells and its inhibition by cocaine. *Synapse* **33:**230–238.

Fischer JF and Cho AK (1979) Chemical release of dopamine from striatal homogenates: evidence for an exchange diffusion model. *J Pharmacol Exp Ther* **208:**203–209.

Foster JD, Pananusorn B, and Vaughan RA (2002) Dopamine transporters are phosphorylated on N-terminal serines in rat striatum. *J Biol Chem* **277:**25178–25186.

Giros B and Caron MG (1993) Molecular characterization of the dopamine transporter. *Trends Pharmacol Sci* **14:**43–49.

Granas C, Ferrer J, Loland CJ, Javitch JA, and Gether U (2003) N-terminal truncation of the dopamine transporter abolishes phorbol ester- and substance P receptor-stimulated phosphorylation without impairing transporter internalization. *J Biol Chem* **278:**4990–5000.

Hénin J, Maigret B, Tarek M, Escrieut C, Fourmy D, and Chipot C (2006) Probing a model of a GPCR/ligand complex in an explicit membrane environment: the human cholecystokinin-1 receptor. *Biophys J* **90:**1232–1240.

Humphrey W, Dalke A, and Schulten K (1996) VMD: visual molecular dynamics. *J Mol Graph* **14:**33–38, 27–28.

Johnson LA, Guptaroy B, Lund D, Shamban S, and Gnegy ME (2005) Regulation of amphetamine-stimulated dopamine efflux by protein kinase Cβ. *J Biol Chem* **280:**10914–10919.

Kantor L and Gnegy ME (1998) Protein kinase C inhibitors block amphetamine-mediated dopamine release in rat striatal slices. *J Pharmacol Exp Ther* **284:**592–598.

Khoshbouei H, Sen N, Guptaroy B, Johnson L, Lund D, Gnegy ME, Galli A, and Javitch JA (2004) N-terminal phosphorylation of the dopamine transporter is required for amphetamine-induced efflux. *PLoS Biol* **2:**E78.

Khoshbouei H, Wang H, Lechleiter JD, Javitch JA, and Galli A (2003) Amphetamine-induced dopamine efflux. A voltage-sensitive and intracellular Na+-dependent mechanism. *J Biol Chem* **278:**12070–12077.

Kitayama S, Shimada S, Xu H, Markham L, Donovan DM, and Uhl GR (1992) Dopamine transporter site-directed mutations differentially alter substrate transport and cocaine binding. *Proc Natl Acad Sci U S A* **89:**7782–7785.

Korkhov VM, Holy M, Freissmuth M, and Sitte HH (2006) The conserved glutamate (Glu136) in transmembrane domain 2 of the serotonin transporter is required for the conformational switch in the transport cycle. *J Biol Chem* **281:**13439–13448.

Lee FJ, Pristupa ZB, Ciliax BJ, Levey AI, and Niznik HB (1996) The dopamine transporter carboxyl-terminal tail. Truncation/substitution mutants selectively confer high affinity dopamine uptake while attenuating recognition of the ligand binding domain. *J Biol Chem* **271:**20885–20894.

Lin Z, Zhang PW, Zhu X, Melgari JM, Huff R, Spieldoch RL, and Uhl GR (2003)

Phosphatidylinositol 3-kinase, protein kinase C, and MEK1/2 kinase regulation of dopamine transporters (DAT) require N-terminal DAT phosphoacceptor sites. *J Biol Chem* **278:**20162–20170.

Loland CJ, Grånäs C, Javitch JA, and Gether U (2004) Identification of intracellular residues in the dopamine transporter critical for regulation of transporter conformation and cocaine binding. *J Biol Chem* **279:**3228–3238.

Loland CJ, Norregaard L, and Gether U (1999) Defining proximity relationships in the tertiary structure of the dopamine transporter. Identification of a conserved glutamic acid as a third coordinate in the endogenous Zn^{2+}-binding site. *J Biol Chem* **274:**36928–36934.

Loland CJ, Norregaard L, Litman T, and Gether U (2002) Generation of an activating Zn^{2+} switch in the dopamine transporter: mutation of an intracellular tyrosine constitutively alters the conformational equilibrium of the transport cycle. *Proc Natl Acad Sci U S A* **99:**1683–1688.

Norregaard L, Frederiksen D, Nielsen EO, and Gether U (1998) Delineation of an endogenous zinc-binding site in the human dopamine transporter. *EMBO J* **17:** 4266–4273.

Phillips JC, Braun R, Wang W, Gumbart J, Tajkhorshid E, Villa E, Chipot C, Skeel RD, Kalé L, and Schulten K (2005) Scalable molecular dynamics with NAMD. *J Comput Chem* **26:**1781–1802.

Pifl C, Agneter E, Drobny H, Sitte HH, and Singer EA (1999) Amphetamine reverses or blocks the operation of the human noradrenaline transporter depending on its concentration: superfusion studies on transfected cells. *Neuropharmacology* **38:** 157–165.

Ramamoorthy S, Samuvel DJ, Buck ER, Rudnick G, and Jayanthi LD (2007) Phosphorylation of threonine residue 276 is required for acute regulation of serotonin transporter by cyclic GMP. *J Biol Chem* **282:**11639–11647.

Rutledge CO (1978) Effect of metabolic inhibitors and ouabain on amphetamine- and potassium-induced release of biogenic amines from isolated brain tissue. *Biochem Pharmacol* **27:**511–516.

Sali A and Blundell TL (1993) Comparative protein modelling by satisfaction of spatial restraints. *J Mol Biol* **234:**779–815.

Saunders C, Ferrer JV, Shi L, Chen J, Merrill G, Lamb ME, Leeb-Lundberg LM, Carvelli L, Javitch JA, and Galli A (2000) Amphetamine-induced loss of human dopamine transporter activity: an internalization-dependent and cocaine-sensitive mechanism. *Proc Natl Acad Sci U S A* **97:**6850–6855.

Scholze P, Nørregaard L, Singer EA, Freissmuth M, Gether U, and Sitte HH (2002) The role of zinc ions in reverse transport mediated by monoamine transporters. *J Biol Chem* **277:**21505–21513.

Sen N, Shi L, Beuming T, Weinstein H, and Javitch JA (2005) A pincer-like configuration of TM2 in the human dopamine transporter is responsible for indirect effects on cocaine binding. *Neuropharmacology* **49:**780–790.

Shi L, Quick M, Zhao Y, Weinstein H, and Javitch JA (2008) The mechanism of a neurotransmitter: sodium symporter–inward release of Na+ and substrate is triggered by substrate in a second binding site. *Mol Cell* **30:**667–677.

Sitte HH, Hiptmair B, Zwach J, Pifl C, Singer EA, and Scholze P (2001) Quantitative analysis of inward and outward transport rates in cells stably expressing the cloned human serotonin transporter: inconsistencies with the hypothesis of facilitated exchange diffusion. *Mol Pharmacol* **59:**1129–1137.

Sitte HH, Huck S, Reither H, Boehm S, Singer EA, and Pifl C (1998) Carrier-mediated release, transport rates, and charge transfer induced by amphetamine, tyramine, and dopamine in mammalian cells transfected with the human dopamine transporter. *J Neurochem* **71:**1289–1297.

Sotomayor M and Schulten K (2004) Molecular dynamics study of gating in the mechanosensitive channel of small conductance MscS. *Biophys J* **87:**3050–3065.

Sulzer D, Sonders MS, Poulsen NW, and Galli A (2005) Mechanisms of neurotransmitter release by amphetamines: a review. *Prog Neurobiol* **75:**406–433.

Thorsness PE and Koshland DE Jr (1987) Inactivation of isocitrate dehydrogenase by phosphorylation is mediated by the negative charge of the phosphate. *J Biol Chem* **262:**10422–10425.

Torres GE (2006) The dopamine transporter proteome. *J Neurochem* **97 (Suppl 1):**3–10.

Uhl GR and Lin Z (2003) The top 20 dopamine transporter mutants: structure-function relationships and cocaine actions. *Eur J Pharmacol* **479:**71–82.

Vaughan RA (2004) Phosphorylation and regulation of psychostimulant-sensitive neurotransmitter transporters. *J Pharmacol Exp Ther* **310:**1–7.

Wu X and Gu HH (2003) Cocaine affinity decreased by mutations of aromatic residue phenylalanine 105 in the transmembrane domain 2 of dopamine transporter. *Mol Pharmacol* **63:**653–658.

Yamashita A, Singh SK, Kawate T, Jin Y, and Gouaux E (2005) Crystal structure of a bacterial homologue of Na^+/Cl-dependent neurotransmitter transporters. *Nature* **437:**215–223.

Zomot E, Bendahan A, Quick M, Zhao Y, Javitch JA, and Kanner BI (2007) Mechanism of chloride interaction with neurotransmitter: sodium symporters. *Nature* **449:**726–730.

Address correspondence to: Dr. Margaret E. Gnegy, Department of Pharmacology, 2220E MSRBIII, University of Michigan Medical School, Ann Arbor, MI 48109-0632. E-mail: pgnegy@umich.edu